Journal of Sound and Vibration (1999) **224**(4), 665–687
Article No. jsvi.1999.2235, available online at http://www.idealibrary.com on IDEAL®

MAPPED INFINITE WAVE ENVELOPE ELEMENTS FOR ACOUSTIC RADIATION IN A UNIFORMLY MOVING MEDIUM

WALTER EVERSMAN

Mechanical and Aerospace Engineering and Engineering Mechanics, University of Missouri-Rolla, Rolla, MO 65401, *U.S.A.*

(*Received* 22 *July* 1998, *and in final form* 22 *January* 1999)

Variable order mapped infinite wave envelope elements are developed for finite-element modelling (FEM) of acoustic radiation in a uniformly moving medium. These elements can be used as a non-reflecting boundary condition for computations on an infinite domain in which a radiating body is immersed in a moving medium which is essentially undisturbed outside of the near field. An additional result of this study shows that the mapped wave envelope elements provide a boundary condition equivalent to stiffness, mass, and damping matrices appended to the inner mesh. By choosing the transition between the standard FEM mesh and the mapped infinite wave envelope as a surface of constant phase the mass matrix is caused to vanish identically. This has implications for transient FEM modelling of acoustic radiation. A demonstration of the characteristics of mapped infinite wave envelope elements is given in the context of acoustic radiation from a turbofan inlet for which benchmark results are known.

1. INTRODUCTION

Modelling of acoustic radiation is usually complicated by the requirement that prediction of the acoustic field is required in some finite subdomain of an infinite domain. This requires that computations be limited to the subdomain with a non-reflecting boundary or that the infinite domain be mapped on to a finite computational domain. In finite element modelling this has led to the study of a number of forms of infinite elements [1–3], wave envelope elements [4, 5], and mapped infinite wave envelope elements [6–9]. The several forms of infinite elements in some sense map the infinite domain to a finite domain. Wave envelope elements restrict computations to a large but finite domain bounded by a Sommerfeld radiation condition. The non-reflecting boundary is reached from an inner standard finite-element domain via large elements in which the shape functions are augmented to reflect decay with distance from the source and the temporal and spatial character of outgoing waves. The attributes of infinite elements and wave envelope elements are combined in mapped infinite wave envelope elements.

0022-460X/99/290665 + 23 $30.00/0

Mapped infinite wave envelope elements have been investigated extensively for acoustic radiation in a stationary medium. They have certain apparent advantages as compared to standard wave envelope elements. In the case of harmonic radiation, the most significant advantage is the possibility of adjusting the order of the elements to fit the requirements of the problem. Formulation of the elements reveals the possibility of including within the element shape function an explicit dependence on inverse powers of the distance from the apparent acoustic source, consistent with theoretical results [8]. This fact allows the introduction of mapped infinite wave envelope elements well into what would normally be considered the acoustic near field, reducing mesh refinement and dimensionality. The shape functions in mapped infinite wave envelope elements can accommodate nearfield effects, and this fact can be enhanced by adjusting the order of the interpolation in the elements to fit the problem requirements. A second advantage in the FEM formulation using the mapped infinite wave envelope elements is that the Sommerfeld radiation boundary is infinitely far away and is never explicitly appended as a natural boundary condition. Astley *et al.* [9] also demonstrated the applicability of mapped infinite wave envelope elements to problems in transient acoustic radiation, a feature which has not been exploited in standard wave envelope elements. With an appropriate choice of mesh geometry they show that mapped infinite wave envelope elements provide a boundary condition which is well suited for time-marching solutions. The advantages of the mapped infinite wave envelope elements are not without cost, and the trade-off comes in the form of increased band width of the discretized field equations that is introduced by high order mapped elements. This may offset efficiency gains achieved by reduction of the extent of the computational near field and therefore the standard FEM mesh if bandwidth-sensitive solvers are used.

The study reported here extends the variable order mapped infinite wave envelope concept to uniform steady flows, principally in connection with aeroacoustic problems related to turbofan acoustic radiation. This is a direct extension of the development of Astley *et al.* [8, 9]. They present their formulation in the context of problems in three dimensions in Cartesian co-ordinates. The application here is in a cylindrical co-ordinate system reduced to two dimensions by taking advantage of periodicity of the solution in the angular co-ordinate. The development of the mapped wave envelope elements is completely general and not restricted to this co-ordinate system. Harmonic radiation is considered explicitly; however it is shown here that as in the case of a stationary medium, with a judicious choice of the mesh geometry, the structure of the mapped elements becomes favorable for transient calculations.

2. AN APPLICATION TO TURBOFAN INLET ACOUSTICS

An important problem of acoustic radiation in a moving medium is available in the study of the acoustic field of a turbofan inlet. The noise due to turbo-machinery sources within the inlet is propagated in the inlet and radiated to the (infinite) far field. Acoustic propagation and radiation occurs in a high-speed potential flow which is the net effect of flow into the inlet and the forward flight of the inlet. In the

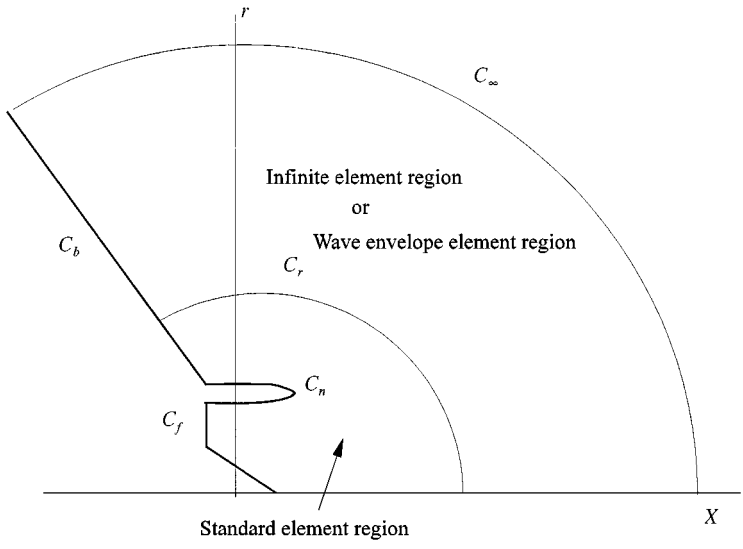

Figure 1. Computational domain showing genetic geometry of the nacelle and boundaries and regions used in the finite element, wave envelope, and mapped infinite wave envelope element formulations.

steady flow far field (perhaps nearer to the inlet than the acoustic far field) acoustic radiation occurs in a uniformly moving medium. It is required to make computations to predict the radiated field in a finite subdomain relatively near the inlet. This has been approached in the past by terminating the computational domain with a Sommerfeld condition on a boundary reached by the use of wave envelope elements [5, 10–12]. Here it is intended to investigate the application of mapped infinite wave envelope elements to obtain closure of the computational domain.

For turbofan inlet acoustic radiation the nacelle geometry and the steady flow field (representing flow into the inlet and forward flight) are assumed to be axially symmetric. The noise source is assumed to be harmonic in time and is decomposed into its angular modal content, allowing a two-dimensional representation of the acoustic field in a plane through the nacelle axis of symmetry. The solution domain is shown in Figure 1. It is the x, r plane in cylindrical co-ordinates. The source plane is designated by C_f. The source is input on this plane by specifying complex amplitudes of incident duct modes [5, 10–12]. The nacelle outer surface is C_n. On this boundary, steady flow and acoustic particle velocities have a vanishing normal component. An artificial baffle C_b formed by a ray from the origin limits the solution domain. The sweep angle is chosen in such a way that minimal effect on the acoustic field is created [13]. The domain of computation is divided into two parts. In an inner region a standard finite-element mesh is used; in the present problem eight-node serendipity elements with the condition that four to five elements per wavelength are required. The near field is terminated on a boundary C_r beyond which farfield elements are used. In previous studies, this region was large but finite and bounded by the surface C_∞, a circle which represents a constant-phase surface

for an acoustic source located at the origin. On this boundary, a radiation condition was specified. Wave envelope elements [5, 10–12] were used in this region. In the present study, the farfield region is extended to infinity and a single layer of mapped infinite wave envelope elements is used to provide a reflection-free boundary on C_r and to compute the acoustic field in the far field as required. The boundary C_∞ is not part of the solution.

3. FINITE ELEMENT FORMULATION

The geometry of the inlet and steady flow field in and around the inlet is axially symmetric. The acoustic field is not axially symmetric but is represented as periodic in a cylindrical co-ordinate system with x being the axis of symmetry, r the cylindrical radius in a circular cross-section at $x = 0$, and θ the angular co-ordinate. Solutions are sought in angular harmonics of a Fourier series enumerated by the angular mode number m. This reduces the solution domain to a two-dimensional x, r plane.

The starting point for the formulation of both the steady mean flow and the acoustic perturbation consists of the inviscid mass and momentum equations and the energy equation in the form of the isentropic equation of state. The acoustic field equations are obtained by considering small perturbations on a steady irrotational mean flow characterized by density ρ_r and speed of sound c_r. This formulation makes it possible to introduce a steady flow velocity potential ϕ_r and an acoustic perturbation velocity potential ϕ. Acoustic perturbations in pressure, density and velocity potential are harmonic in time with frequency η_r and harmonic in the angular co-ordinate θ of the form $p(x, r)e^{i(\eta_r t - m\theta)}$, $\rho(x, r)e^{i(\eta_r t - m\theta)}$, $\phi(x, r)e^{i(\eta_r t - m\theta)}$. In linearized form, the weak formulation is [5, 10–12]

$$\int\int_V \int \{\nabla W \cdot (\rho_r \nabla\phi + \rho \nabla\phi_r) - i\eta_r W \rho\} \, dV = \int_S \int W(\rho_r \nabla\phi + \rho \nabla\phi_r) \cdot \mathbf{n} \, dS \quad (1)$$

The weighting functions are taken as $W(x, r, \theta) = W(x, r)e^{im\theta}$. Angular harmonics proportional to $e^{-im\theta}$ represent the decomposition of the solution periodic in θ in a Fourier series. The angular mode number m is a parameter of the solution. The surface integral is over all surfaces bounding the domain. The unit normal for the surface integral is out of the domain at the surface in question. The weak formulation continues with the linearized momentum equation

$$\rho = -\frac{\rho_r}{c_r^2}(i\eta_r \phi + \nabla\phi_r \cdot \nabla\phi) \quad (2)$$

which is used to replace ρ in equation (1). The linearized equation of state,

$$p = c_r^2 \rho, \quad (3)$$

is used to produce an alternative form of the momentum equation in terms of acoustic pressure,

$$p = -\rho_r(\mathrm{i}\eta_r\phi + \nabla\phi_r \cdot \nabla\phi). \tag{4}$$

The acoustic particle velocity and acoustic velocity potential are related according to

$$\mathbf{v} = \nabla\phi. \tag{5}$$

The linearization process also produces the weighted residual formulation for the steady flow,

$$\iiint_V \nabla W \cdot (\rho_r \nabla\phi_r)\,\mathrm{d}V = \int_S \int W(\rho_r \nabla\phi_r)\cdot \mathbf{n}\,\mathrm{d}S, \tag{6}$$

and the steady flow momentum equation in terms of the speed of sound,

$$c_r^2 = 1 - \frac{(\gamma - 1)}{2}[\nabla\phi_r \cdot \nabla\phi_r - M_\infty^2], \tag{7}$$

and in terms of the steady flow density,

$$\rho_r = \left[1 - \frac{(\gamma - 1)}{2}(\nabla\phi_r \cdot \nabla\phi_r - M_\infty^2)\right]^{1/(\gamma-1)}. \tag{8}$$

Equations (1)–(8) are in non-dimensional form where ϕ is the acoustic potential, ϕ_r is the local mean flow (reference) potential, ρ is the acoustic density, ρ_r is the local mean flow density, p is the acoustic pressure, and c_r is the local speed of sound in the mean flow. All quantities are made non-dimensional by using the density in the far field, ρ_∞, the speed of sound in the far field, c_∞, and a reference length which is defined as the duct radius at the source plane, R, where acoustic modal amplitudes are defined. This plane could be the fan plane or the exit guide vane plane, but it is not restricted to these locations. The acoustic potential is non-dimensional with respect to $c_\infty R$, and the acoustic pressure with respect to $\rho_\infty c_\infty^2$. Lengths are made non-dimensional with respect to R. Time is scaled with R/c_∞, leading to the definition of non-dimensional frequency $\eta_r = \omega R/c_\infty$; ω is the dimensional source frequency. $M_\infty = M_o$ is the Mach number in the far field representing the forward flight effect.

Equation (6) is the weighted residual formulation for the calculation of the compressible potential flow within and around the nacelle. Equations (7) and (8) are subsidiary relations that can be used in an iterative solution which at each stage uses a density field derived from the previous iteration step. $\nabla\phi_r$, c_r, ρ_r are required data for the weighted residual formulation of the acoustic problem. In the results reported here only the first iteration of this process is used to define the potential

flow field. This is accomplished by solving the incompressible problem and then computing a variation in steady flow density and speed of sound.

The surface integral in equation (1) provides the boundary conditions on the duct walls, and at the source. The acoustic source is specified by the complex amplitudes of acoustic duct modes at the source plane. On this plane, the FEM nodal value of acoustic potential are replaced by the complex amplitudes of the acoustic potential modes by an eigenfunction expansion. The incident acoustic modal amplitudes are input and the reflected modal amplitudes are computed as part of the solution. Details of this procedure are available in [5, 10–12].

A previous study [13] shows that the baffle can be positioned to produce practically no effect on typical acoustic radiation patterns. Therefore, there is no contribution from the surface integral on the baffle. In previous studies, the surface integral provided the mechanism for enforcing the Sommerfeld radiation condition on C_∞. In the present application of mapped wave envelope elements the surface integral is never explicitly introduced on a far-field boundary because the assumed form of the solution in the outer region implicitly satisfies the Sommerfield condition.

In terms of acoustic potential the weak formulation is, from equations (1) and (2),

$$\int\int_V \int \frac{\rho_r}{c_r^2}\{c_r^2\,\nabla W\cdot\nabla\phi-(\mathbf{M}_r\cdot\nabla W)(\mathbf{M}_r\cdot\nabla\phi)+\mathrm{i}\eta_r[W(\mathbf{M}_r\cdot\nabla\phi)-(\mathbf{M}_r\cdot\nabla W)\phi]$$

$$-\eta_r^2 W\phi\}\,\mathrm{d}V=\int_S\int\frac{\rho_r}{c_r^2}\{c_r^2 W\,\nabla\phi-\mathbf{M}_r W(\mathbf{M}_r\cdot\nabla\phi)-\mathrm{i}\eta_r\mathbf{M}_r W\phi\}\cdot\mathbf{n}\,\mathrm{d}S, \quad (9)$$

where the local non-dimensional steady flow velocity is $\mathbf{M}_r=\nabla\phi_r$. Equation (9) is the weak formulation in the entire domain, however in the steady flow far field it simplifies considerably with the steady flow given by $\mathbf{M}_r=M_0 i$ and $\rho_r=1$, $c_r=1$. Furthermore, the surface integral on C_∞ has no contribution in the formulation proposed here because there is no longer any surface on which a Sommerfeld radiation condition is to be applied. The weak formulation in the steady flow far field is

$$\int\int_V\int\left\{\nabla W\cdot\nabla\phi-M_0^2\frac{\partial W}{\partial x}\frac{\partial\phi}{\partial x}+\mathrm{i}\eta_r M_0\left(W\frac{\partial\phi}{\partial x}-\frac{\partial W}{\partial x}\phi\right)-\eta_r^2 W\phi\right\}\mathrm{d}V=0. \quad (10)$$

In the cylindrical co-ordinate system used here, some liberty is taken in defining the gradient operations as

$$\nabla W=\frac{\partial W}{\partial x}\mathbf{i}+\frac{\partial W}{\partial r}\mathbf{e}_r+\frac{\mathrm{i}m}{r}W\mathbf{e}_\theta, \quad \nabla\phi=\frac{\partial\phi}{\partial x}\mathbf{i}+\frac{\partial\phi}{\partial r}\mathbf{e}_r-\frac{\mathrm{i}m}{r}\phi\mathbf{e}_\theta, \quad (11,12)$$

and suppressing factors $e^{\pm im\theta}$ which arise as part of the weighting and trial functions as explained in connection with equation (1). These factors cancel throughout all of the products in equations (9) and (10). Equations (11) and (12) reflect the harmonic angular dependence of ϕ and W. The non-dimensional velocity M_0 in equation (10) is the Mach number of the forward flight.

In the steady flow near field, where the flow is non-uniform, equation (9) is discretized using standard finite-element techniques. Example calculations presented in this study are based on two-dimensional rectangular isoparametric serendipity elements with eight nodes.

In the steady flow far field where the flow is essentially uniform, equation (10) can be discretized using wave envelope elements or by introducing mapped infinite wave envelope elements to obtain closure of the computational domain. It is the formulation in terms of mapped wave envelope elements which is of interest here.

4. THE INFINITE MAPPING

Because of the harmonic dependence on the angle θ the originally three-dimensional weak formulation reduces to two spatial co-ordinates x and r. The x, r plane is shown in Figure 1 where the boundary C_r separates an interior region in which standard FEM descretization is used from an outer region in which mapped wave envelope elements are used. The exterior region must be in the steady flow far field. Figure 2 shows an element in the outer region in the x–r plane of the cylindrical co-ordinate system. The element is bounded by the surface C_r on which

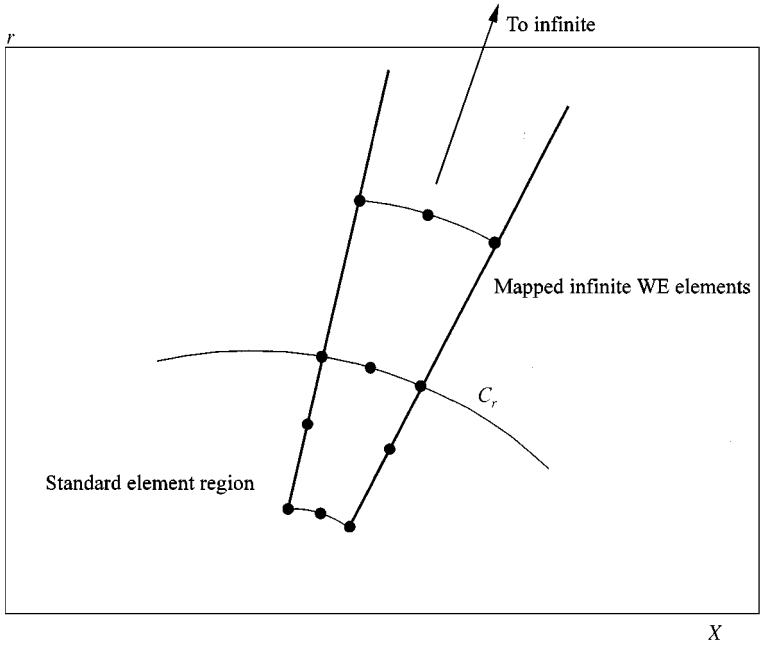

Figure 2. Details of the finite/infinite-element interface.

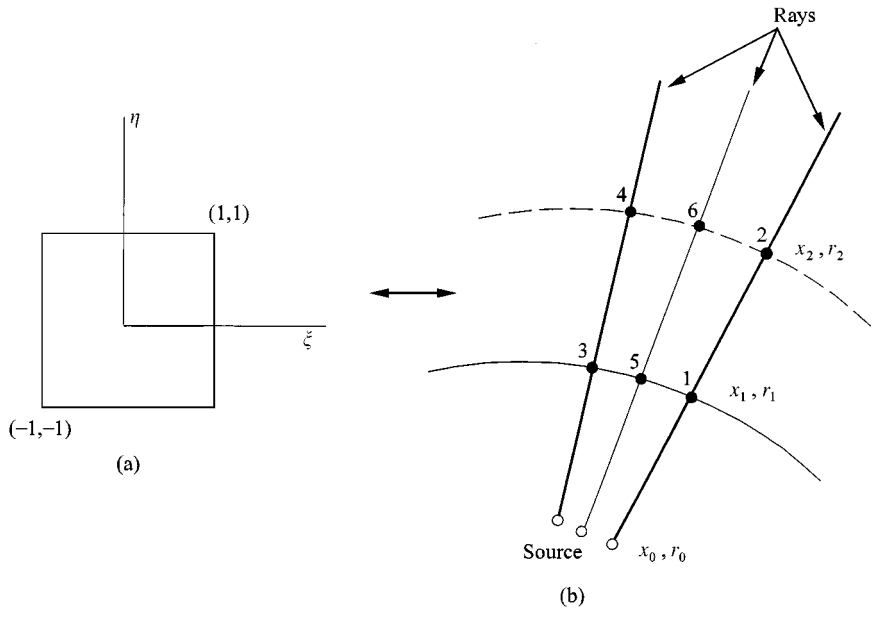

Figure 3. Geometric details of the mapping between the infinite element and the parent element: (a) parent element, (b) mapped wave envelope (WE) element.

it conform with an element of the conventional mesh. The edges of the element are straight lines, extending outward more or less radially, though not necessarily from the axis system origin nor necessarily from a common origin. For the elements used in this investigation which conform with eight-node serendipity elements in the conventional mesh (each with three nodes on C_r), a third radial line between the two edges is required. For simplicity, each of the three straight lines will be referred to as rays. In Figure 1, the outer surface C_∞ is the notional outer boundary of the element at infinity. A ray of an element has an apparent origin at a point x_0, r_0 which in general can be different for each ray. The element maps to a parent element in the ξ, η plane, $-1 \leqslant \xi \leqslant 1$, $-1 \leqslant \eta \leqslant 1$, as shown in Figure 3. The rays of the element map to the ξ axis with $\eta = -1, 0, 1$ in the parent element according to

$$x = \frac{-2\xi}{1-\xi} x_1 + \frac{1+\xi}{1-\xi} x_2, \quad r = \frac{-2\xi}{1-\xi} r_1 + \frac{1+\xi}{1-\xi} r_2, \tag{13, 14}$$

Since

$$\frac{-2\xi}{1-\xi} + \frac{1+\xi}{1-\xi} = 1, \tag{15}$$

the mapping is unchanged by an origin shift. Therefore, it can also be used to yield a mapping relative to the source at x_0, r_0:

$$x - x_0 = \frac{-2\xi}{1-\xi}(x_1 - x_0) + \frac{1+\xi}{1-\xi}(x_2 - x_0), \tag{16}$$

$$r - r_0 = \frac{-2\xi}{1-\xi}(r_1 - r_0) + \frac{1+\xi}{1-\xi}(r_2 - r_0). \tag{17}$$

The node x_1, r_1 is defined by the requirement that the element conform with the conventional element on the boundary C_r. A particularly useful form of the mapping is obtained if the node at x_2, r_2 is located such that $x_2 - x_0 = 2(x_1 - x_0)$ and $r_2 - r_0 = 2(r_1 - r_0)$. This makes the mapping simplify to

$$x - x_0 = \frac{2(x_1 - x_0)}{1-\xi}, \qquad r - r_0 = \frac{2(r_1 - r_0)}{1-\xi}. \tag{18}$$

The mapping has the properties that $\xi = -1$ maps to $x - x_0 = x_1 - x_0$, $r - r_0 = r_1 - r_0$, $\xi = 0$ maps to $x - x_0 = 2(x_1 - x_0)$, $r - r_0 = 2(r_1 - r_0)$, and $\xi = 1$ maps to $x - x_0 = \infty, r - r_0 = \infty$. The mapping along a "ray" transforms the infinite domain in the physical co-ordinates to the domain $-1 \leqslant \xi \leqslant 1$ in the parent element. The inverse mapping is

$$\xi = 1 - \frac{2(x_1 - x_0)}{x - x_0}, \qquad \xi = 1 - \frac{2(r_1 - r_0)}{r - r_0}. \tag{19}$$

It is easily deduced that this mapping along a "ray" also applies for the polar radius of the point x, r relative to $x_0, r_0, r_p = \sqrt{(x - x_0)^2 + (r - r_0)^2}$, in the form

$$r_p = \frac{2\sqrt{(x_1 - x_0)^2 + (r_1 - r_0)^2}}{1-\xi} = \frac{2r_{p_1}}{1-\xi} \tag{20}$$

and

$$\xi = 1 - 2r_{p_1}/r_p. \tag{21}$$

This form emphasizes the role of the base node x_0, r_0 as a "source" for the "ray" and the distance r_p as the polar distance from the source.

The infinite-element mapping is completed by a conventional mapping on $-1 \leqslant \eta \leqslant 1$. The element shown in Figure 3 has six nodes numbered as shown. Nodes 1–4 are corner nodes and nodes 5 and 6 are mid-side nodes on C_r and C_2 (the locus of the nodes x_2, r_2). The mapping is of the form

$$x = [M(\xi, \eta)]\mathbf{x}, \quad r = [M(\xi, \eta)]\mathbf{r}, \tag{22}$$

where $[M(\xi, \eta)]$ is a row vector of six shape functions $M_i(\xi, \eta)$ and $\mathbf{x}, \mathbf{r}$ are vectors of nodal values of x, r. With the nodal numbering scheme used in Figure 3 the explicit

form of the shape function is

$$M_1(\xi,\eta) = 0{\cdot}5\eta(\eta-1)\frac{-2\xi}{1-\xi}, \qquad M_2(\xi,\eta) = 0{\cdot}5\eta(\eta-1)\frac{1+\xi}{1-\xi},$$

$$M_3(\xi,\eta) = 0{\cdot}5\eta(\eta+1)\frac{-2\xi}{1-\xi}, \qquad M_4(\xi,\eta) = 0{\cdot}5\eta(\eta+1)\frac{1+\xi}{1-\xi},$$

$$M_5(\xi,\eta) = (1-\eta)(1+\eta)\frac{-2\xi}{1-\xi}, \qquad M_6(\xi,\eta) = (1-\eta)(1+\eta)\frac{1+\xi}{1-\xi}. \tag{23}$$

The mapping described here is simply another view of the results presented by Astley *et al.* [8] specialized to the cylindrical co-ordinate system.

In preparation for development of a mapped infinite wave envelope element for a uniformly flowing medium it can also be noted that the results of equations (16)–(21) can be extended to other "distances" along a ray yielding a similar mapping. For example

$$R = \sqrt{(x-x_0)^2 + \beta^2(r-r_0)^2} = \frac{2R_1}{1-\xi}, \tag{24}$$

where $R_1 = \sqrt{(x_1-x_0)^2 + \beta^2(r_1-r_0)^2}$ and $\beta^2 = 1-M^2$ and M is the Mach number of the uniformly flowing medium. A second useful mapping is

$$\psi = \frac{1}{\beta^2}[-M(x-x_0)+R] = \frac{2\psi_1}{1-\xi}, \tag{25}$$

where $\psi_1 = (1/\beta^2)[-M(x_1-x_0)+R_1]$. These observations are important to the extension of the application of the mapped infinite wave envelope element to acoustic radiation in uniform steady flow.

5. SOURCE SOLUTION IN UNIFORM FLOW

The weak formulation of equation (10) for acoustic radiation in a uniformly moving medium is consistent with the differential equation

$$\left(\frac{\partial}{\partial t} + M\frac{\partial}{\partial x}\right)^2 \phi = \nabla^2\phi. \tag{26}$$

A fundamental harmonic source solution for this equation is

$$\phi = \mathrm{e}^{\mathrm{i}\eta_r t}\frac{\mathrm{e}^{(-\mathrm{i}\eta_r/\beta^2)(-Mx+\sqrt{x^2+\beta^2r^2})}}{\sqrt{x^2+\beta^2r^2}}, \tag{27}$$

where $\beta = \sqrt{1 - M^2}$ and $r^2 = y^2 + z^2$. This can be verified by direct substitution or by noting that the transformation of variables

$$x' = \frac{x}{\beta}, \quad r' = r, \quad t' = \frac{M}{\beta}x + \beta t \tag{28}$$

reduces the convected wave equation (26) to the standard wave equation

$$\partial^2\phi/\partial t'^2 = \nabla'^2\phi \tag{29}$$

in the transformed variables which has a fundamental harmonic source solution

$$\phi = \mathrm{e}^{\mathrm{i}\frac{\eta_r}{\beta}t'} \frac{\mathrm{e}^{-\mathrm{i}\frac{\eta_r}{\beta}\sqrt{x'^2 + r'^2}}}{\sqrt{x'^2 + r'^2}}. \tag{30}$$

Equation (27) is then obtained replacing the change of variables of equation (28). In terms of the definitions of equations (24) and (25), the fundamental harmonic source solution for source location at x_0, r_0 is

$$\phi = \mathrm{e}^{\mathrm{i}\eta_r t} \frac{\mathrm{e}^{-\mathrm{i}\eta_r\psi}}{R}. \tag{31}$$

6. SHAPE FUNCTIONS IN THE INFINITE ELEMENTS

Shape function in the mapped infinite wave envelope elements can be constructed to display the characteristics of the fundamental source solution at large distances from the source in the form

$$\phi = Q(\mathbf{x})\mathrm{e}^{-\mathrm{i}m\theta} R_1 \frac{\mathrm{e}^{-\mathrm{i}\eta_r(\psi(\mathbf{x}) - \psi_1)}}{R(\mathbf{x})} = P(\mathbf{x})\mathrm{e}^{-\mathrm{i}m\theta}\mathrm{e}^{-\mathrm{i}\mu(\mathbf{x})}, \tag{32}$$

where the notation $\mathbf{x} = (x, r)$ and $\mu(\mathbf{x}) = \eta_r(\psi(\mathbf{x}) - \psi_1)$ is used and is similar to the notation used by Astley *et al.* [8]. $\mu(\mathbf{x})$ is the phase relative to the surface C_r separating the infinite-element region from the region of standard FEM interpolation and ψ_1 emphasizes that this phase is dependent on the specific "ray" on which equation (32) is evaluated. ψ_1 would be a constant for the entire infinite-element region if C_r is a surface of constant ψ (a "constant-phase surface"), but in general would vary from node to node on C_r. The most direct way to make ψ_1 invariant for the mesh is to construct the mesh so that for all infinite elements x_0, r_0 (the "source point") is common and C_r is a surface of constant ψ ("phase") relative to the common "source". The mesh used by Eversman *et al.* [5, 10–12] has this property (x_0, r_0 are at the mesh origin) and is used in examples in this investigation. At large R, equation (32) should have asymptotic behavior in R consistent with equation (31). The function $P(\mathbf{x})$ should therefore display the

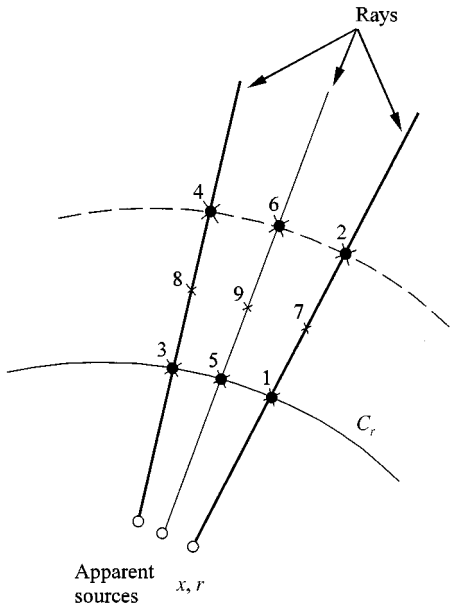

Figure 4. Example of an infinite element with nine × interpolation nodes and six ● mapping nodes. This element produces an asymptotic interpolation in the far field of third order in R_1/R.

appropriate asymptotic behavior in R, should be capable of accounting for nearfield effects, and should interpolate in the standard FEM context in the η co-ordinate in the parent element.

In terms of ξ, η co-ordinates of the parent element, $\mu(\mathbf{x})$ and $R(\mathbf{x})/R_1$, have simple forms suggested by equations (24) and (25);

$$\mu(\xi, \eta) = \psi_1 \frac{1+\xi}{1-\xi}, \quad \frac{R_1}{R(\xi, \eta)} = \frac{1}{2}(1-\xi). \tag{34, 35}$$

In equation (34), ψ_1 can be a function of η on the inner boundary of the element $\xi = -1$, interpolated relative to nodal values on C_r. The function $Q(\mathbf{x})$ in equation (32) which accounts for nearfield behavior in the infinite element can be represented by a standard FEM interpolation

$$Q(\xi, \eta) = [S(\xi, \eta)]\underline{Q}, \tag{36}$$

where $\underline{Q}$ is a vector of nodal values of $Q(\mathbf{x})$. There are six nodes involved in the infinite mapping and these can be used as nodes in the interpolation of $Q(\mathbf{x})$. It will generally be appropriate to use more than the mapping nodes by including extra nodes along the rays as shown in Figure 4 which demonstrates the introduction of one extra node midway between the mapping nodes on each ray and suggests a convenient nodal numbering scheme.

The shape functions for the element shown in Figure 4 with the additional node midway between the mapping nodes on a given ray are based on nine-node Lagrangian interpolation with the extra nodes mapped to $\xi = -\frac{1}{3}$. In general, $P(\mathbf{x})$

is interpolated within an element according to

$$P(\xi, \eta) = [N(\xi, \eta)]\underline{Q}, \tag{37}$$

where the shape function $N_i(\xi, \eta)$, the shape function corresponding to node i, is constructed from the mth-order Lagrangian shape function for node i, $L_i^p(\xi, \eta)$, according to

$$P_i(\xi, \eta) = N_i(\xi, \eta) = \tfrac{1}{2}(1 - \xi)L_i^p(\xi, \eta). \tag{38}$$

Some liberty is taken with notation here; $L_i^p(\xi, \eta)$ is defined so that p is the order of interpolation (number of nodes) along the ξ-axis. Along the η-axis the order conforms with the order used in the standard FEM region, which is 3 in the two-dimensional serendipity elements implemented in the model reported here. It is interesting to note that $N_i(\xi, \eta)$ is unity only for nodes with $\xi = -1$ (the Lagrangian interpolation functions have the value unity for all nodes). The vector of nodal values $\underline{Q}$ corresponding to the evaluation of $Q(\mathbf{x})$ only corresponds to nodal value of $P(\mathbf{x})$ for nodes on the surface C_r. Because of this, and because of the phase term $e^{-i\mu(\mathbf{x})}$ in equation (32), which is unity only on the surface C_r, in the infinite elements the solution vector does not correspond to nodal values of acoustic potential at most of the nodes. The potential can be easily reconstructed by postprocessing.

The form of the shape functions defined by equation (38) can be interpreted in global co-ordinate by using equation (24) to show that

$$1 - \xi = 2(R_1/R), \quad \xi = 1 - 2(R_1/R). \tag{39}$$

Equations (38) and (39) suggest that the shape functions in global co-ordinates along a ray are of the form

$$P_i(x, r) = \gamma_1(R_1/R) + \gamma_2(R_1/R)^2 + \gamma_3(R_1/R)^3 + \cdots + \gamma_n(R_1/R)^n, \tag{40}$$

n is determined from the order of Lagrangian interpolation. For a p node interpolation leading to polynomials in ξ of degree $p - 1$ it is determined that $n = p$. A similar result was shown in the case of radiation in a stationary medium [8].

Reference to "variable order" mapped infinite wave envelope elements relates to the choice of the order of the Lagrangian interpolation and therefore to the powers of R_1/R in the asymptotic expansion for the shape function. Conceptually this could be extended to any order, but as pointed out by Astley *et al.* [8] there is a limit imposed by the onset of numerical problems probably related to ill conditioning if the order is too high.

7. WEIGHT FUNCTIONS IN THE INFINITE ELEMENTS

Astley *et al.* [8] show that in order for the boundary integral introduced in the weak formulation to have no contribution on the boundary at infinity it is necessary for the weighting functions to be functions of $\{R_i/R(\mathbf{x})\}^{q+1}$, with $q > 1$.

The weight functions are of the form

$$\phi = Q(\mathbf{x})\mathrm{e}^{\mathrm{i}m\theta}\left(\frac{R_1}{R(\mathbf{x})}\right)^{q+1}\mathrm{e}^{\mathrm{i}\eta_r(\psi(\mathbf{x})-\psi_1)} = D(\mathbf{x})P(\mathbf{x})\mathrm{e}^{\mathrm{i}m\theta}\,\mathrm{e}^{\mathrm{i}\mu(\mathbf{x})} \tag{41}$$

where

$$D(\mathbf{x}) = (R_i/R(\mathbf{x}))^q \tag{42}$$

In the parent element,

$$D(\xi, \eta) = (1/2)^q(1-\xi)^q \tag{43}$$

The weight functions are the complex conjugates of the shape functions multiplied by the additional decay term. In the present investigation $q = 3$. The notation here has been chosen to correspond to that used by Astley *et al.* [8] to emphasize the similarity with their development in the case of a stationary medium. Only the details hidden in the definitions of ψ and R are different.

8. THE WEAK FORMULATION IN THE INFINITE-ELEMENT REGION

The weak formulation of equation (10) for the infinite-element region in which the steady flow is necessarily uniform is obtained by using equations (32) and (43) defining the assumed form of solution and the weight functions in the infinite-element region. The gradient operations on the assumed shape and weighting functions yield

$$\nabla\phi = (\nabla P - \mathrm{i}\eta_r \mathrm{P}\nabla\mu)\mathrm{e}^{-\mathrm{i}\eta_r\mu} \tag{44}$$

and

$$\nabla W = (D\nabla P^* + \mathrm{i}\eta_r \mathrm{D}\mathrm{P}\nabla\mu + P\nabla D)\mathrm{e}^{\mathrm{i}\eta_r\mu}, \tag{45}$$

where the notation

$$\nabla P = \frac{\partial P}{\partial x}\mathbf{i} + \frac{\partial P}{\partial r}\mathbf{e}_r - \frac{\mathrm{i}m}{r}P\mathbf{e}_\theta, \quad \nabla P^* = \frac{\partial P}{\partial x}\mathbf{i} + \frac{\partial P}{\partial r}\mathbf{e}_r + \frac{\mathrm{i}m}{r}P\mathbf{e}_\theta \tag{46, 47}$$

is used as in equations (11) and (121) because of the factors $\mathrm{e}^{\pm \mathrm{i}m\theta}$ which are suppressed. By using standard finite-element operations, equation (11) can be formulated at the global level to yield complex element "stiffness" matrices $[\tilde{K}_{ij}]$ defined in terms of real mass, stiffness and damping matrices,

$$[\tilde{K}_{ij}] = -\eta_r^2[M_{ij}] + \mathrm{i}\eta_r[\mathrm{C}_{ij}] + [\mathrm{K}_{ij}], \tag{48}$$

where

$$K_{ij} = \int\int_V \int \left\{ D\left[(1-M^2)\frac{\partial P_i}{\partial x}\frac{\partial P_j}{\partial x} + \frac{\partial P_i}{\partial r}\frac{\partial P_j}{\partial r} + \frac{m^2}{r^2} P_i P_j \right] \right.$$

$$\left. + P_i\left[(1-M^2)\frac{\partial D}{\partial x}\frac{\partial P_j}{\partial x} + \frac{\partial D}{\partial r}\frac{\partial P_j}{\partial r} \right] \right\} \mathrm{d}V, \tag{49}$$

$$M_{ij} = \int\int_V \int DP_iP_j \left\{ 1 - \left[(1-M^2)\left(\frac{\partial \mu}{\partial x}\right)^2 + \left(\frac{\partial \mu}{\partial r}\right)^2 + 2M\frac{\partial \mu}{\partial x} \right] \right\} \mathrm{d}V \tag{50}$$

$$C_{ij} = \int\int_V \int \left\{ DP_i\left[(1-M^2)\frac{\partial \mu}{\partial x}\frac{\partial P_j}{\partial x} + M\frac{\partial P_i}{\partial x} + \frac{\partial \mu}{\partial r}\frac{\partial P_j}{\partial r} \right] \right.$$

$$- D\left[(1-M^2)\frac{\partial \mu}{\partial x}\frac{\partial P_i}{\partial x} + M\frac{\partial P_j}{\partial x} + \frac{\partial \mu}{\partial r}\frac{\partial P_i}{\partial r} \right] P_j$$

$$\left. - \left[(1-M^2)\frac{\partial D}{\partial x}\frac{\partial \mu}{\partial x} + M\frac{\partial D}{\partial x} + \frac{\partial D}{\partial r}\frac{\partial \mu}{\partial r} \right] P_iP_j \right\} \mathrm{d}V. \tag{51}$$

The definitions of the stiffness, mass, and damping matrices of equations (49)–(51) are implemented at the element level using the infinite mapping to the parent element. These results reduce to those of Astley *et al.* [8] when the medium is stationary and when account is taken of the operations which are particular to the cylindrical co-ordinate system. It is not difficult to generalize to a three-dimensional Cartesian co-ordinate system.

9. AN IMPORTANT PROPERTY OF THE MASS MATRIX

The mass matrix of equation (50) vanishes if the surface C_r separating the standard finite-element region from the infinite-element region is a surface of constant phase for an apparent acoustic source location x_0, r_0 which is common for all elements. This is shown by referring to the definition of $\mu(\mathbf{x})$,

$$\mu(\mathbf{x}) = \eta_r(\psi(\mathbf{x}) - \psi_1), \tag{52}$$

where

$$\psi(\mathbf{x}) = (1/\beta^2)[-M(x-x_0)+R], \quad R = \sqrt{(x-x_0)^2 + \beta^2(r-r_0)^2}. \tag{53, 54}$$

Since it is stipulated that C_r is a constant phase surface, it follows that ψ_1 is constant. The apparent source location is the same for all elements, leading to the conclusion that x_0, r_0 are constants. It can then be verified that

$$(1-M^2)(\partial\mu/\partial x)^2 + (\partial\mu/\partial r)^2 + 2M(\partial\mu/\partial x) = 1 \tag{55}$$

which from equation (50) leads to the result

$$M_{ij} = 0. \tag{56}$$

This is consistent with the findings of Astley *et al.* [8] in the case of a stationary medium when the surface C_r is a sphere, a constant-phase surface in this case. While of some interest in the time harmonic formulation considered here, the vanishing of the mass matrix is of central importance when a time-dependent formulation is implemented in the stationary medium case. It remains to be established that this is equally important in the case of a uniformly moving medium.

10. TURBOFAN INLET EXAMPLE

Figure 1 shows the generic geometry of a turbofan inlet in an x, r plane of a cylindrical co-ordinate system. The nacelle interior and exterior shape are typical of realistic nacelles. The acoustic source is on the plane C_f and produces a combination of radial modes at a specified angular mode m and non-dimensional frequency η_r. The source strength is specified by the complex mode amplitudes. This type of source would correspond to rotor alone noise or rotor/exit guide vane interaction noise. The frequency is determined by the number of blades on the rotor and the angular mode number by the rotor and exit guide vane blade counts. The nacelle has a forward velocity specified by the Mach number M_0, which is represented for the stationary nacelle by a steady flow directed toward the nacelle. The steady flow into the nacelle is specified by the Mach number M_i, taken to be uniform on the source plane. The steady flow field inside and outside the nacelle, computed on the FEM acoustic mesh, provides input data for the FEM acoustic calculations. This mesh is over refined for the steady flow calculations but this inefficiency is more than offset by the convenience of input data on a mesh compatible with the acoustic mesh.

The details of the FEM acoustic computations with the domain closed by a conventional wave envelope transition region to a Sommerfeld radiation boundary are given in references [5, 10–12]. In this example the propagation and radiation problem is formulated with the standard FEM treatment in the steady flow near field and the domain is closed in the far field by the use of mapped infinite wave envelope elements. The specific case shown is at a reduced frequency $\eta_r = 25$ and angular mode $m = 23$ with only the first radial mode incident. Only one radial mode propagates and it has a cutoff ratio near unity, which indicates that the peak lobe of the radiation pattern will be at a high angle relative to the nacelle axis. In this case it is over 60° to the nacelle axis for the case of $M_i = 0{\cdot}20$ and $M_0 = 0{\cdot}30$. Figure 5 shows the standard mesh in the region which has been abritrarily declared as the steady flow near field. The steady flow far field is where the flow is essentially the $M_0 = 0{\cdot}3$ uniform flow. The outer boundary of this mesh is the surface C_r and it is a circle of constant phase for a source at the axis system origin. The infinite-element region is outside of C_r and not shown. The same inner mesh was used with the outer region consisting of seven layers of standard wave envelope elements extending to 10 duct radii ahead of the inlet for the purpose of producing

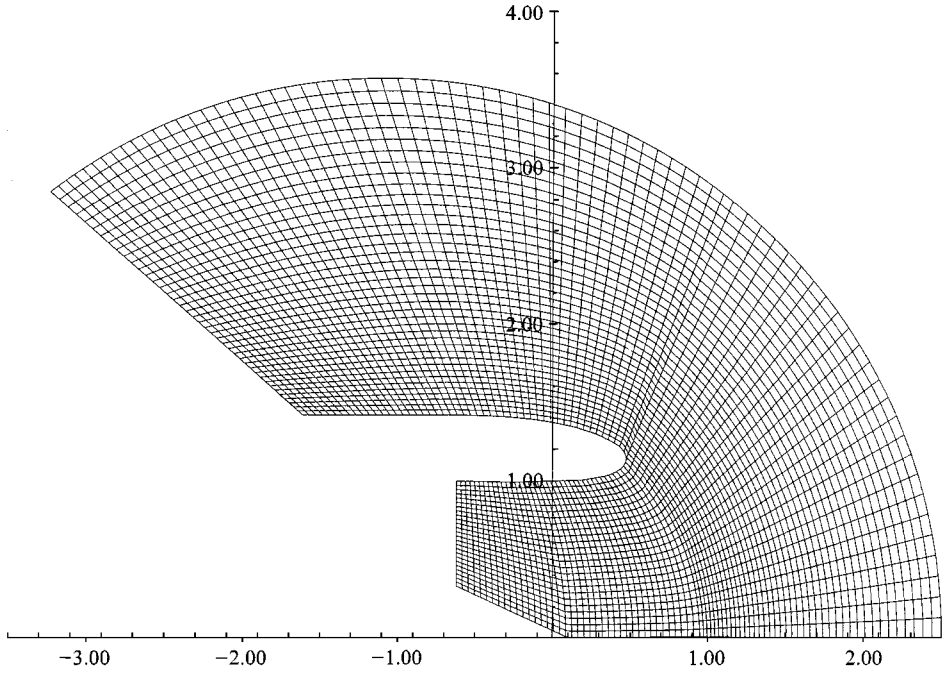

Figure 5. The nearfield mesh of standard finite elements bounded by the surface C_r.

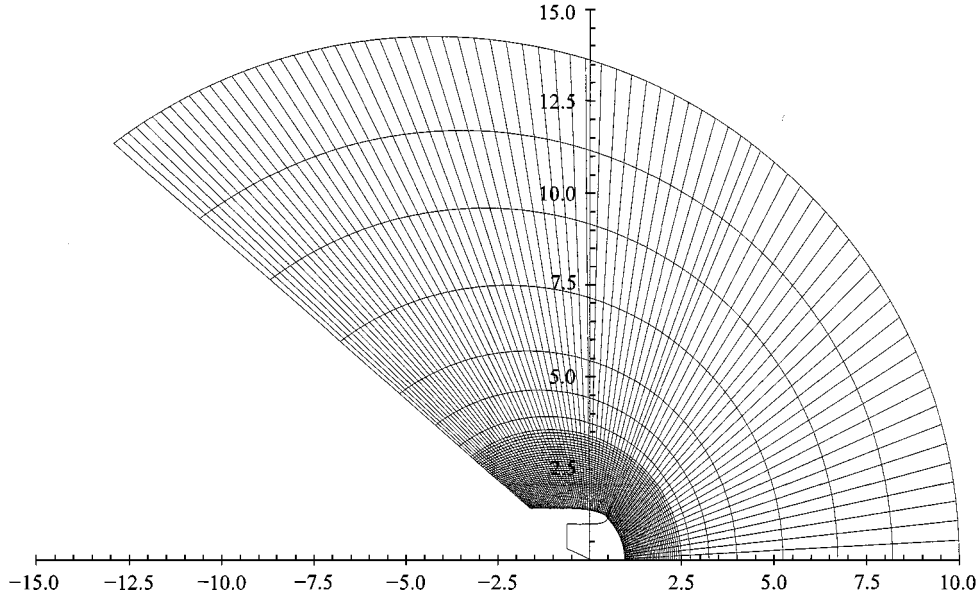

Figure 6. Standard wave envelope mesh used in finite element/wave envelope element formulation.

comparison results. The outer mesh for this case is shown in Figure 6. The standard code has been extensively benchmarked by experiment [12] and by comparison with available approximate analytical results. Numerical experiments have shown that for this frequency radiated fields are particularly difficult to model.

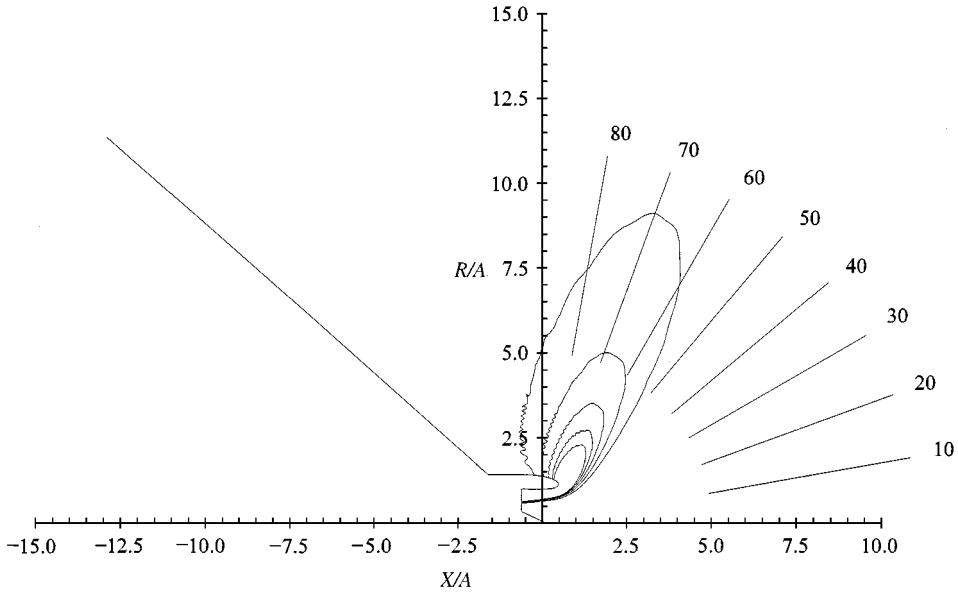

Figure 7. Contours of equal acoustic potential in the entire computational domain for the finite-element/wave envelope element formulation. External mach number $M_0 = 0{\cdot}3$, source plane Mach number $M_i = 0{\cdot}2$, non-dimensional frequency $\eta_r = 25$, angular mode number $m = 23$, first radial mode.

At high angles to the axis the source is certainly not seen as a simple source on C_r as located in this example. It is reasonable to expect that non-reflecting boundary behavior based on an asymptotic approximation representing a simple source would be difficult to achieve.

The results which will be displayed are contours of constant acoustic potential magnitude in an x, r plane superposed on the nacelle geometry. Acoustic potential has been chosen since there is an extra post-processing step to obtain acoustic pressure which introduces its own potential for error, unrelated to the details of the reflection free boundary. Post-processing for pressure in the standard FEM region involve the same operations whether standard wave envelope or mapped infinite wave envelope elements are used in the outer solution. Figure 7 shows the radiation pattern generated by using the standard code (wave envelope elements) and plotting contours of constant acoustic potential in the entire computational domain. Figure 8 shows the same results limited to the region of standard finite elements, which provides a more detailed way of viewing the reflection free performance of the boundary C_r. Figure 9 shows the results when mapped infinite wave envelope elements are used to provide a reflection free boundary. In the case shown the formulation is based on eight-node Lagrangian interpolation in the mapped elements in the ξ direction (eight nodes). This corresponds to introducing R_1/R in the expansion for asymptotic behavior of the farfield solution up to the eighth power [refer to equation (40)]. Element integration is based on 9×3 Gauss points. It was found that five-node Lagrangian interpolation (powers of R_1/R up to five in the asymptotic expansion) was not sufficient.

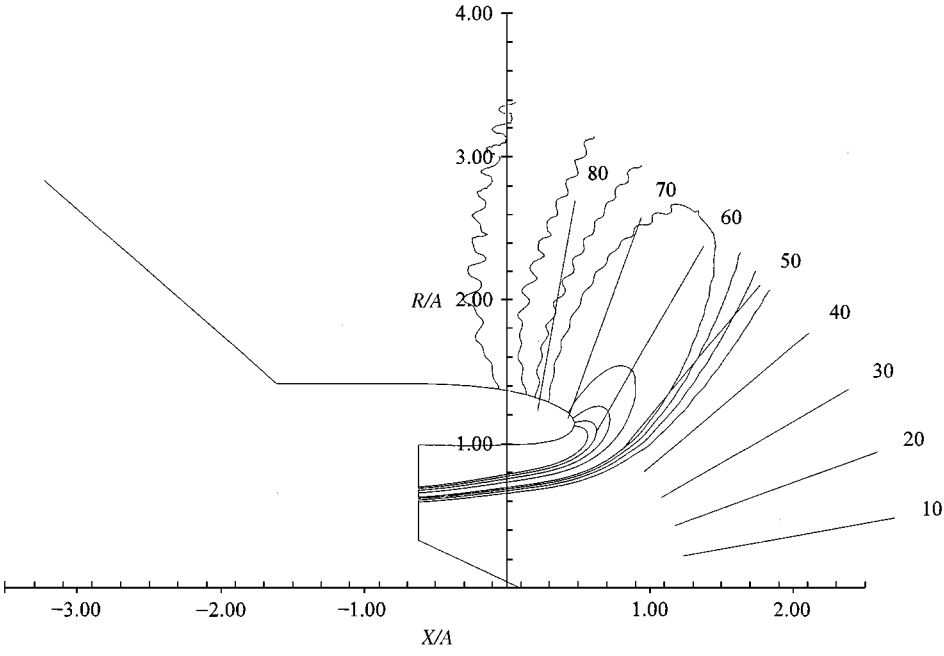

Figure 8. Contours of equal acoustic potential in the standard finite-element region for the finite-element/wave envelope element formulation. External mach number $M_0 = 0{\cdot}3$, source plane Mach number $M_i = 0{\cdot}2$, non-dimensional frequency $\eta_r = 25$, angular mode number $m = 23$, first radial mode.

Figure 7 displaying the entire solution field to the Sommerfeld boundary (10 duct radii of the nacelle axis) suggests significant reflection from the boundary which appears in the waviness of the contours, particularly at higher angles where diffraction around the inlet lip is important and where the nacelle surface interferes with the radiation. The quality of the solution does not improve with the further mesh refinement, indicating that the mesh is suitable for the frequency. Figure 8 zooms in on the region inside C_r and the poor quality of the solution is apparent. In Figure 9 the same level contours are considerably less ragged, indicating that reflection has been essentially eliminated. It is of interest to recall that the computational domain includes the artificial baffle C_b and it appears that it has little effect on the radiated field, consistent with the results reported in reference [13].

The clear conclusion is that poor quality of the solution when standard wave envelope elements are used is due to the inability of the wave envelope elements to provide a completely reflection-free boundary for the complicated source configuration and this location of C_r. In principle expanding C_r should improve the wave envelope element performance, but this has the obvious implication of directly increasing the dimensionality (presuming it is required that the mesh refinement is retained) and the hidden implication of requiring even further mesh refinement due to the growth in element aspect ratio as C_r is expanded.

Variable order mapped infinite wave envelope elements generally will increase the maximum bandwidth of the mesh (the inner mesh may have eight nodes per

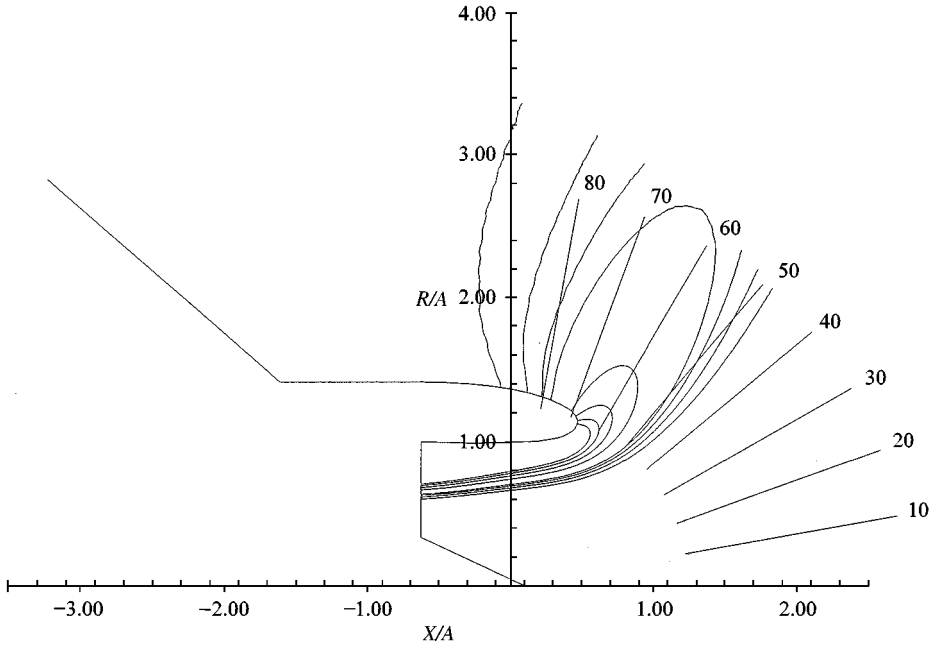

Figure 9. Contours of equal acoustic potential in the standard finite-element region for the finite-element/mapped infinite wave envelope element formulation. External mach number $M_0 = 0{\cdot}3$, source plane Mach number $M_i = 0{\cdot}2$, non-dimensional frequency $\eta_r = 25$, angular mode number $m = 23$, first radial mode. The order of the interpolation in the infinite elements is eighth power in R_i/R.

element and the single infinite element layer has been tested here with as many as 24 nodes per element). In frontal solvers, this tends to slow down the solution even if the total number of nodes is more or less the same in the mapped elements as in the standard wave envelope elements. In the example discussed, a frontal solver is used and the mapped infinite-element computation have an execution time which is in a ratio of about 7/5 compared to the standard wave envelope code. This cost is not unimportant, but must be assessed against the requirements for solution quality. In this case, the infinite-element results are clearly superior.

The question now arises; how much can the computational domain be reduced by using the infinite elements to enhance the reflection-free boundary? To partly address the question, the boundary C_r has been reduced to a radius of two duct radii ahead of the origin. Note in the original mesh of Figure 5 the mesh extends 2·5 duct radii ahead of the origin. In order to maintain approximately the same mesh refinement, the element count between the "highlight circle" (a circle passing through the tip of the inlet lip and intersecting the axis near $r = 1$) has been reduced from 50 to 35. Figure 10 shows acoustic potential level curves in the standard element region for the case using mapped wave envelope elements for closure. The quality of the solution is still substantially superior to that seen in Figure 8 for which closure was achieved using regular wave envelope elements (note that the level curves are not the same in Figures 8 and 10 because they are based on the maximum level on C_r, which differs because C_r differs). The

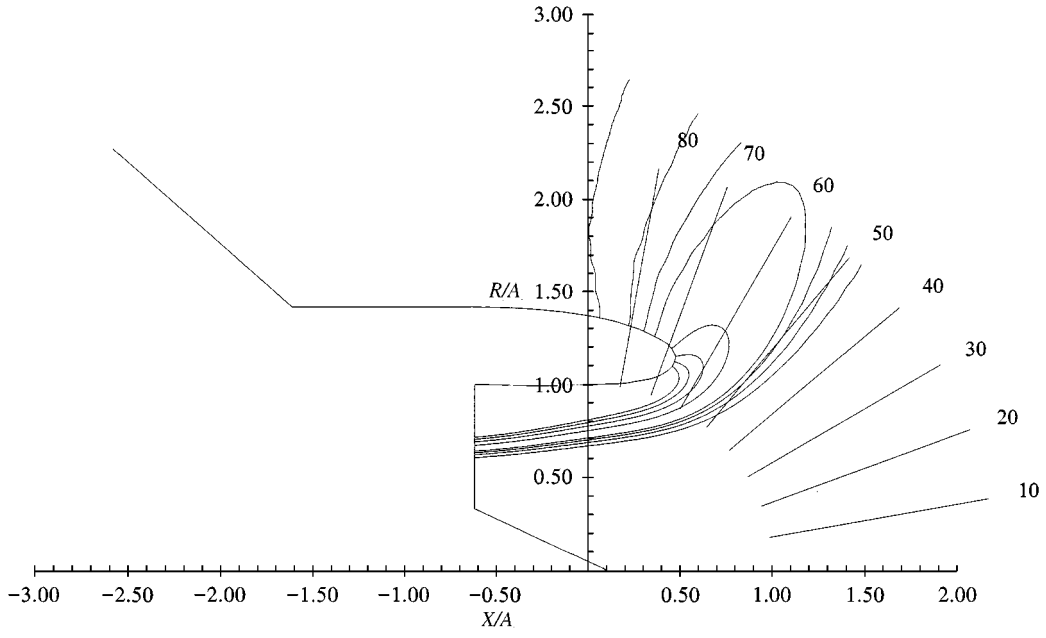

Figure 10. Contours of equal acoustic potential in the standard finite-element region for the finite-element/mapped infinite wave envelope element formulation on a reduced mesh in the standard element region. External mach number $M_0 = 0{\cdot}3$, source plane Mach number $M_i = 0{\cdot}2$, non-dimensional frequency $\eta_r = 25$, angular mode number $m = 23$, first radial mode. The order of the interpolation in the infinite elements is eighth power in R_i/R.

computation time ratio is now nearly 1/1 and the mapped infinite-element results are still superior.

11. CONCLUSION

It has been shown that with suitable modifications mapped infinite wave envelope elements can be used to provide an effective reflection-free boundary for acoustic radiation in a uniform steady flow. The adaptation of the elements to this case is based on the observation that all important "distances" along "rays" map to the parent element in the infinite mapping in exactly the same way. This permits the fundamental solution for radiation from a source in uniform flow to be mapped to the parent element in a form similar to the mapping in the case of a stationary medium. The fundamental solution forms the basis for an asymptotic expansion in R^{-n} in the infinite elements, where R is the "convected radius", $R^2 = x^2 + \beta^2 r^2$. The order of the asymptotic expansion can be chosen to meet the needs of the problem. Element mapping functions are identical to those previously proposed for the stationary medium case and the shape functions are of the same form as those in the stationary medium case with differences only in the details.

Computational examples have been based on acoustic radiation from a turbofan inlet which has been the subject of several previous investigations in which an FEM model was developed with the reflection-free closure of the computational domain

based on standard wave envelope elements. Examples have shown that mapped infinite wave envelope elements provide a superior reflection-free boundary for cases in which the standard wave envelope elements generate reflections which appear in the radiated field. It should be noted that the improved performance may not be without cost. If relatively high order mapped elements (asymptotic behavior to R^{-n} where n is relatively large) are required, the maximum front width of the FEM formulation may be larger than would occur in the standard wave envelope element formulation. For frontal solvers this may decrease computational efficiency. However, this cost has a substantial benefit in the quality of the solution which may not be achievable with the standard wave envelope elemnts without expanding the boundary between standard FEM and the wave envelope element region. In fact, it has been shown that by taking advantage of the reduction in size of the inner region (standard element region) which is achievable with mapped infinite elements it is possible to obtain superior solutions without increasing computation time.

It has been found that the mapped infinite wave envelope element region can be cast in the form of appended mass, damping and stiffness matrices. With a suitable choice of the surface which separates the standard FEM region from the infinite-element region and the restriction that the mapping and shape functions in the infinite elements are based on a common apparent source location, it has been shown that the element mass matrices vanishe. This has previously been shown to be important for transient FEM formulations for radiation in a stationary medium. This suggests that similar investigations should be carried out in the case of uniform external flow.

ACKNOWLEDGMENTS

The work reported here was supported in part by NASA Lewis Research Center under Grant NAG3-2109. Initial stages of the investigation were carried out while the author was an Erskine Fellow in the Department of Mechanical Engineering at the University of Canterbury, Christchurch, New Zealand. Discussions with Professor R. J. Astley were invaluable.

REFERENCES

1. P. BETTESS 1997 *International Journal for Numerical Methods in Engineering* **11**, 53–64. Infinite elements.
2. O. C. ZIENKIEWWICZ, K. BANDO, P. BETTES, C. EMSON and T. C. CHIAM 1985 *International Journal for Numerical Methods in Engineering* **21**, 1229–1251. Mapped infinite elements for exterior wave problems.
3. D. S. BURNETT and R. L. HOLFORD 1998 *Computer Methods in Applied Mechanics and Engieering* **164**, 49–76. An ellipsoidal acoustic infinite element.
4. R. J. ASTLEY and W. EVERSMAN 1983 *Journal of Sound and Vibration* **88**, 47–64. Finite element formulations for acoustical radiation.
5. A. V. PARRETT and W. EVERSMAN 1986 AIAA Journal **24**, 753–759. Wave envelope and finite element approximations for turbofan noise radiation in flight.
6. R. J. ASTLEY and G. J. MACAULAY 1994 *Journal of Sound and Vibration* **170,** 97–118. Mapped wave envelope elements for acoustical radiation and scattering.

7. L. CREMERS and K. R. FYFE 1995 *Journal of the Acoustical Society of America* **97**, 2028–2040. On the use of a variable order infinite wave envelope element for acoustic radiation and scattering.
8. R. J. ASTLEY, G. J. MACAULAY, J.-P. COYETTE and L. CREMERS 1998 *Journal of Acoustical Society of America* **103**, 49–63. Three dimensional wave envelope elements of variable order for acoustic radiation and scattering. Part I. Formulation in the frequency domain.
9. R. J. ASTLEY, J-P. COYETTE and L. CREMERS 1998 *Journal of the Acoustical Society of America* **103**, 64–72. Three dimensional wave envelope elements of variable order for acoustic radiation and scattering. Part II. Formulation in the time domain.
10. W. EVERSMAN, A. V. PARRETT, J. S. PREISSER and R. J. SILCOX 1985 *ASME Journal of Vibration, Acoustics, Stress, and Reliability in Design* **107**, 216–223. Contributions to the finite element solution of the fan noise radiation problem.
11. I. DANDA ROY and W. EVERSMAN 195 *ASME Journal of of Vibration and Acoustics* **117**, 109–115. Improved finite element modeling of the turbofan engine inlet radiation problem.
12. J. S. PREISSER R. J. SILCOX, W. EVERSMAN and A. V. PARRETT 1985 *Journal of Aircraft* **22**, 57–62. Flight study of induced turbofan inlet acoustic radiation with theoretical comparisons.
13. W. EVERSMAN and I. DANDA ROY 1998 *AIAA Paper 98-2250, AIAA/CEAS 4th Aeroacoustics Conference*, 2–4 June, 1998, *Toulouse, France*. The effect of a baffle on acoustic radiation directivity.